Compression of Oceanic Lithosphere: An Analysis of Intraplate Deformation in the Central Indian Basin

MARIA T. ZUBER[1]

Department of Geological Sciences, Brown University, Providence, Rhode Island

Intraplate compressional deformation in the Central Indian Basin is expressed as linear E-W trending topographic undulations and geoid anomlies with characteristic spacings of approximately 200 km. To elucidate the nature of this deformation, we develop models of an oceanic lithosphere in a state of horizontal compression. The lithosphere is treated as a viscous or plastic layer of uniform strength which overlies a viscous half space in which strength decreases exponentially with depth. We compare models in which deformation with a dominant wavelength develops in response to flexural buckling and the hydrodynamic growth of instabilities. For the viscous flexural buckling model, deformation is constrained to occur in the antisymmetric mode by flexural folding, which is characterized by uniform bending of the layer. In the hydrodynamic flow model a range of deformational styles are possible. In a strong viscous lithosphere, deformation of the layer occurs by flexural folding at a wavelength which agrees with that predicted from flexural buckling theory. In a lithosphere of intermediate strength, the layer deforms by folding characterized by thickening which localizes beneath topographic highs. In a relatively weak lithosphere, the layer incurs an even greater amount of localized thickening and deforms in the symmetric or pinch-and-swell mode by inverse boudinage. If the layer has a plastic rheology, deformation occurs by inverse boudinage independent of the yield stress. Results from models in which the layer folds either flexurally or with periodic thickening are consistent with the observed depth distribution of seismicity in the Central Indian Basin and with experimental rock rheological data. Because of the trade-off between buoyancy forces and layer strength in determining the dominant wavelength, a lithosphere which was overlain by weak sediments when intraplate deformation initiated can be characterized by a compressive layer strength almost a factor of 3 less than a lithosphere which was initially sediment-free. For a range of plausible models which consider both a sediment-covered and sediment-free lithosphere, the observed wavelength requires deviatoric stresses in the Indian plate of several hundreds of MPa.

INTRODUCTION

One of the fundamental assumptions in plate tectonics is that lithospheric plates behave rigidly, except along their boundaries. As most global dynamic and kinematic tectonic models are formulated on the basis of this assumption, it is of obvious importance to characterize and understand those areas in which plates are deforming internally. The rigid plate hypothesis is most notably violated in the Central Indian Basin in an area, shown in Figure 1, which is bounded on the west by the Chagos-Laccadive Ridge and on the east by the Sunda Arc, and extends southward beyond the distal edges of the Bengal and Nicobar Fans. Intraplate deformation consists of approximately E-W trending topographic undulations with spacings in the range 100–300 km and amplitudes of 1–3 km [*Weissel et al.*, 1980]. Prominent geoid anomalies with amplitudes of approximately 2 m and free-air gravity anomalies with magnitudes ranging from 30 to 80 mGal correlate with the basement deformation [*Weissel et al.*, 1980]. On the basis of an unconformity in a sedimentary section of the Bengal Fan, *Weissel et al.* [1980] suggested that deformation commenced in the late Miocene, approximately coincident with the Himalayan orogeny. The age of oceanic lithosphere at the onset of deformation was in the approximate range 40–70 Ma. On the basis of relative plate motion analyses, *Wiens et al.* [1985] suggested that this area is a diffuse boundary between the Indo-Arabian and Australian plates.

[1] Now at Geodynamics Branch, NASA Goddard Space Flight Center, Greenbelt, Maryland.

In contrast to most intraplate regions, the Central Indian Basin exhibits a high degree of seismicity [*Sykes*, 1970; *Stein and Okal*, 1978; *Bergman and Solomon*, 1980, 1985; *Wiens et al.*, 1985]. *Bergman and Solomon* [1985] used the most comprehensive set of intraplate focal mechanisms yet assembled for this region and found the direction of maximum compressive stress to be approximately N10°W. This is consistent with numerical models of intraplate stresses formulated for assumed distributions of plate boundary forces [*Richardson et al.*, 1979; *Cloetingh and Wortel*, 1985]. Seismic reflection profiles of the area [cf. *Weissel et al.*, 1980; *Geller et al.*, 1983] show that extensive high-angle faulting disrupts the oceanic crust and overlying sediments. The faulting is pervasive and is not confined to either crests or troughs in the basement topography. The average strike of the faults is about N100°E [*Weissel et al.*, 1980], approximately normal to the direction of maximum compressive stress. This suggests that faulting is predominantly reverse in nature; however, the absence of shallow seismicity [*Bergman and Solomon*, 1985] and the difficulty in measuring displacement directions of faults visible on seismic reflection records lend some uncertainty to this interpretation.

Intraplate deformation in the Central Indian Basin has previously been modeled in terms of flexural buckling of an elastic or elastic-plastic plate. The observed wavelength of deformation requires an elastic plate thickness of 12 km [*Weissel et al.*, 1980], which is more than a factor of 2 less than that predicted by observations of flexure [e.g., *Bodine et al.*, 1981]. The buckling stress for a 12-km-thick elastic plate is 2400 MPa, which is in excess of the compressive strength of the lithosphere as suggested by experiments [e.g., *Goetze and Evans*, 1979; *Kirby*, 1983]. Flexural buckling of an elastic-plastic plate, with an effective thickness corresponding to the
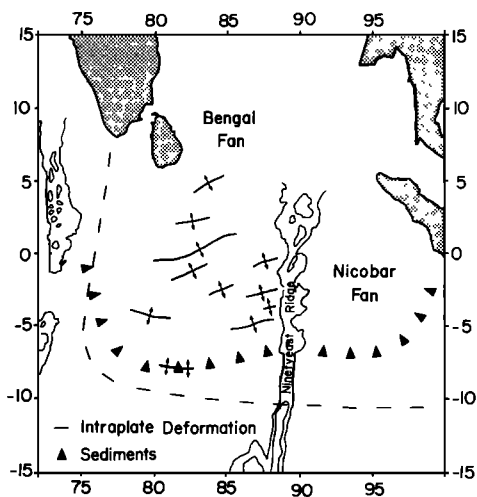
Fig. 1. Location map of the Central Indian Basin. Triangle apices indicate the approximate southern limit of sediments from the Bengal and Nicobar Fans. Dashed curve represents the western and southern extent of the observed intraplate deformation [after Geller et al., 1983]. Note that deformation occurs in regions not overlain by sediments. Implications are discussed in the text. Locations of the most prominent ridges are shown by solid curves with anticline symbols.

age of the lithosphere at the onset of intraplate deformation, occurs at a wavelength of about 200 km and at a buckling stress of about 600 MPa [McAdoo and Sandwell, 1985].

In this study, we investigate the regular development of intraplate structure in the Central Indian Basin through models in which deformation arises due to flexural buckling and the hydrodynamic growth of instabilities, with emphasis on the latter. Details of these models are based on two aspects of the intraplate deformation that were not considered in previous studies. (1) The magnitude of the stress required for elastic buckling in combination with the high degree of intraplate seismicity and pervasive near-surface faulting observed in the Central Indian Basin provide compelling evidence that deformation throughout the lithosphere in this area occurs nonelastically. We therefore model the lithosphere using viscous and plastic rheologies. In these models we take into account the effect of cooling of the oceanic lithosphere with age in determining its rheological structure. (2) The flexural models described previously as well as that examined in this study contain thin plate approximations in which shear stresses due to vertical loading are assumed to be insignificant in magnitude in comparison to bending stresses. As a consequence these models treat only the antisymmetric (folding) mode of deformation. In the hydrodynamic flow formulation the effects of shear stresses are incorporated, and as a result, a range of deformational styles, including flexure, are possible. We compare the flexural and hydrodynamic flow models in order to assess the conditions under which thin plate approximations can be reasonably invoked in models of large-scale lithospheric compression.

MODELS

Viscous Flexure

A thin plate approach is employed to evaluate the dominant wavelength and growth rate for buckling of a viscous layer. In order to approximate the temperature dependence of flow in the weak lower lithosphere, the layer is underlain by a fluid substrate in which viscosity decreases exponentially with

depth. As is illustrated in Figure 2, the plate is subjected to a horizontal end load and a vertical bottom load. Inherent assumptions are that the flexural wavelength is much greater than the plate thickness and that bending stresses associated with flexure are greatly in excess of accompanying shear stresses.

The governing equation for flexural buckling of a non-linear viscous layer of thickness h is [cf. Timoshenko and Woinowsky-Krieger, 1959]

$$D\dot{w}^{iv} + \bar{\sigma}_{xx}hw'' + \Delta\rho g w = \tilde{\sigma}_{zz} \qquad (1)$$

where a prime indicates a partial derivative with respect to x, an overdot represents a partial derivative with respective to time, $\Delta\rho$ is the difference in density between the materials above and below the layer, $\bar{\sigma}_{xx}$ is the horizontal normal stress due to the uniform compression, $\tilde{\sigma}_{zz}$ is the vertical normal stress exerted on the bottom of the layer by the viscous substrate,

$$D = \mu_l h^3/3n \qquad (2)$$

is the flexural rigidity of a layer with viscosity μ_l evaluated at $\bar{\sigma}_{xx}$, and n is the exponent in the stress-strain rate relationship. The density below the layer is taken to be that of the mantle. Above the layer, the densities of both water and sediments are considered in order to assess the possible role of the Bengal and Nicobar Fans in influencing the deformation during its early stages. The sediment cover is treated as a weak fluid beneath which basement folds develop which does not contribute to the strength of the lithosphere. The vertical velocity in the layer is expressed

$$w = A \sin kx \qquad (3)$$

where A is the amplitude and k is the wave number. The normal load due to the flow in the substrate has the form

$$\tilde{\sigma}_{zz} = -2\mu_s(k)\dot{A}k \sin kx \qquad (4)$$

where $\dot{A}$ is the time rate of change of the amplitude. The substrate viscosity μ_s, which relates individual harmonics of normal stress and vertical velocity, is wave number-dependent.
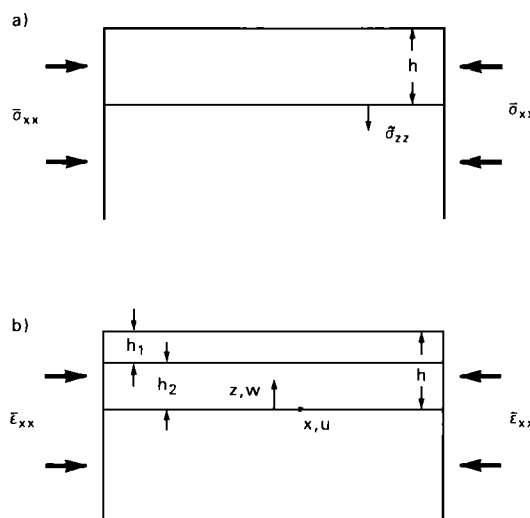

Fig. 2. Models of oceanic lithosphere for (a) viscous flexure and (b) hydrodynamic flow formulations. In the hydrodynamic flow model the upper layer represents oceanic crust and the lower layer and half space correspond to strong and weak regions of the upper mantle, respectively. The thickness of the strong layer of the lithosphere h equals the sum of the crustal h_1 and mantle h_2 layer thicknesses.

If the strength in the substrate is uniform, then μ_s is constant. For a substrate in which strength decreases exponentially with depth, as in the present problem, $\mu_s(k) \simeq \mu_l$ as $k \to \infty$ and $\mu_s(k) \simeq 0$ as $k \to 0$. By substituting (3) and (4) into (1), the rate of amplitude growth can be expressed

$$\frac{\dot{A}}{A} = \frac{k^2 \bar{\sigma}_{xx} h - \Delta\rho g}{k(k^3 D + 2\mu_s)} \tag{5}$$

By substituting $S = \Delta\rho g h/(\bar{\sigma}_{xx}/2)$ and the stress-strain rate relationship $\sigma = 4\mu_l \varepsilon$ into (5), the flexural growth rate factor q_f can be written

$$q_f = \frac{12[(kh)^2 - 2S]}{kh[(kh)^3 + 24\mu_s/\mu_l]} \tag{6}$$

The dominant wavelength of viscous flexural buckling occurs at the wave number at which q_f is a maximum.

Hydrodynamic Flow

In this formulation the "strong layer" of the lithosphere consists of two layers, each of uniform strength. As is shown in Figure 2, the top and bottom layers correspond, respectively, to the crust and that part of the underlying mantle which is capable of supporting appreciable deviatoric stresses. As both the brittle and ductile regimes contribute significantly to the depth-integrated strength of the lithosphere (compare Figure 7), both plastic and viscous rheologies are considered for the layers. Viscous behavior is assumed for the substrate. In the plastic model the layers are assigned identical rheologies, while in the viscous model the layers differ in terms of the experimental flow laws used to represent the respective rheologies of the crust and mantle. Both crust-water and crust-sediment density contrasts are considered. As for the flexural buckling model, the sediment cover is treated as a strengthless fluid. The hydrodynamic flow model also incorporates the effect of the density constrast at the Moho; however, the results shown later are essentially insensitive to geologically reasonable variations of this parameter.

Details of the theoretical formulation for the unstable growth of perturbations in a horizontally stressed, viscosity-stratified model lithosphere are presented by *Fletcher and Hallet* [1983], *Zuber et al.* [1986], and *Ricard and Froidevaux* [1986]. Deformation during lithospheric compression arises due to the amplification of small random disturbances at the free-surface and along subsurface interfaces between layers of differing mechanical properties. The total flow in the medium is expressed mathematically as the sum of a perturbing flow which describes the growth of initial disturbances and the basic state of uniform shortening [e.g., *Fletcher*, 1977; *Smith*, 1975, 1977].

In determining the perturbing flow beneath the layer, the thermal structure of the oceanic lithosphere due to cooling with age is considered. The effective viscosity in the substrate takes the form

$$\bar{\mu}(z) = \mu_0 e^{z/\zeta} \tag{7}$$

where μ_0 is the viscosity at the mantle layer-substrate interface $[\mu_0 = \mu(z = 0)]$; ζ is the viscosity decay length; and z is depth measured negative downward. The temperature $T(z)$ in the substrate is determined from a standard half space cooling model [*Davis and Lister*, 1974], which for the present geometry is written

$$T(z) = T_s + (T_m - T_s) \operatorname{erf}[(h - z)/2(\kappa t')^{1/2}] \tag{8}$$

where T_s and T_m are the surface and mantle temperatures, respectively; h is the strong layer thickness; κ is the thermal diffusivity; and t' is the age of the lithosphere at the onset of deformation. The substrate viscosity is expressed in the desired form by substituting (8) and the constitutive relationship for steady state ductile flow into (7), and defining $\bar{\mu}(z)$ and $d\bar{\mu}/dz$ at the layer-substrate interface so that

$$\mu_0 = \frac{\exp[Q/(n_3 R_g T)]}{2(A^*)^{1/n_3}\bar{\varepsilon}_{xx}^{(1-1/n_3)}} \tag{9}$$

$$\zeta = \frac{(\pi\kappa t')^{1/2} n_3 R_g T^2}{Q(T_m - T_s)\exp\{-[h/2(\kappa t)^{1/2}]^2\}} \tag{10}$$

where A^*, n_3, and Q are the preexponential frequency factor, stress exponent, and activation energy in the flow law of the substrate, and R_g is the gas constant. In terms of the viscosity and the mean horizontal strain rate $\bar{\varepsilon}_{xx}$, which is defined to be positive in compression, the strength at the top of the substrate is

$$\tau_0 = 2\mu_0\bar{\varepsilon}_{xx} \tag{11}$$

The solution of a linear system of equations for the stress and velocity matching conditions and the rate of amplitude growth at each interface in the model lithosphere yields the perturbing flow during the initial stages of deformation [cf. *Fletcher and Hallet*, 1983]. The component of the vertical velocity which contributes to instability growth has the form

$$w = W(k, z)\cos kx \tag{12}$$

where $W(k, z)$ satisfies the incompressibility condition and continuity equations.

In a compressional instability, the shape of an ith perturbed interface at time t is represented by a superposition of Fourier harmonics

$$\delta_i(x, t) = \sum_k A_i(k, t)\sin kx \tag{13}$$

where δ_i and A_i are interface shapes in the spatial and wave number domains, respectively. The amplitude of a perturbation at a given time can be shown to have the form

$$A_i(k, t) = A_i(k, 0)\exp\{(1 + q)\bar{\varepsilon}_{xx}t\} \tag{14}$$

where $A_i(k, 0)$ is the initial amplitude; $\bar{\varepsilon}_{xx}t$ is the mean horizontal strain, and q is the growth rate. The dominant wavelength $\lambda_d(=2\pi/k_d)$ is defined by the wave number k_d at which the growth rate is maximized (q_d).

The parameter $S = (\rho_1 - \rho_0)gh/\tau$ controls the relative contribution of the buoyancy force due to topographic variations to the stress required to deform the strong layer at a prescribed strain rate. The parameter $\alpha = \zeta/h$, which controls the viscous dissipation in the substrate, is the ratio of the decay depth of the substrate viscosity to the strong layer thickness. The parameter $R = \tau_1/\tau_2$ is the ratio of crustal to mantle layer strength. Both a strong layer of uniform strength $(R = 1)$ and a mantle layer which is stronger than the overlying crustal layer are considered.

Results

Comparison of Models

Figure 3 shows growth rate spectra for the flexural and hydrodynamic flow models plotted as a function of dimensionless wave number and wavelength for a range of S. Both models assume a layer and substrate with a Newtonian $(n = 1)$
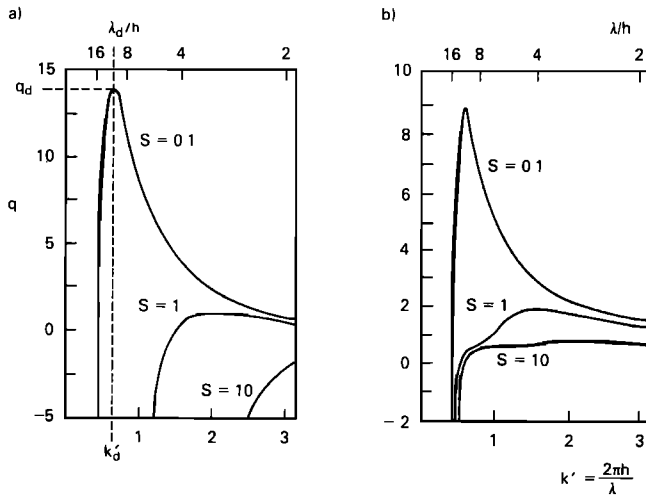
Fig. 3. Growth rate spectra for (a) viscous flexure and (b) hydrodynamic flow models for a range of S values. The dominant wave number k_d' and wavelength λ_d correspond to the maximum growth rate q_d for a given value of S. For $S = 0.1$ the dominant wavelengths are in good agreement. At larger S the dominant wavelengths deviate, indicating the breakdown of the thin plate approximations in the flexural buckling theory. Values of $\alpha = 0.1$ and $n = 1$ for the layer and substrate were assumed for both models. For the hydrodynamic flow model $R = 1$.

rheology and $\alpha = 0.1$. The diagram illustrates how S affects the magnitude q_d and position k_d' or λ_d/h of the maximum growth rate. For increasing S both models exhibit (1) broadening of the peak of the growth rate spectrum, (2) increasing stability, and (3) decreasing dominant wavelength. For $S = 0.1$ both models show a relatively strong instability over a narrow range of wave numbers. For $S = 10$ only the hydrodynamic flow model exhibits a maximum growth rate. However, this peak occurs over such a wide range of wave numbers that it is questionable whether unstable deformation would develop at a discrete wavelength.

The $S = 0.1$ cases illustrate the excellent agreement of the dominant wave numbers for large λ_d/h. The progressively greater disagreement of the models with decreasing λ_d/h indicates the breakdown of the thin plate approximations in the flexural buckling theory. Figure 3 demonstrates that if deformation is characterized by large λ_d/h, then either the flexural buckling or hydrodynamic flow model can be used to relate the observed wavelength to the mechanical structure of the medium. In the Central Indian Basin, the occurrence of intraplate earthquakes with focal depths as great as 40 km (see Figure 7) suggests that the assumption of a thin plate may not be applicable in modeling this region. We therefore use the more general hydrodynamic flow model to further investigate the nature of intraplate deformation.

Properties of Hydrodynamic Flow Model

Figure 4 shows the relationship between q_d, S, and α for a model lithosphere with a viscous layer. Small S, which corresponds to a strong layer, and small α, which reflects a small amount of viscous dissipation in the substrate, favor instability. The model lithosphere is unstable for the entire range of both S and α. This is in contrast to a medium in extension, which can be stable for sufficiently large values of these parameters [*Fletcher and Hallet*, 1983]. The fact that a compressing medium is theoretically unstable does not guarantee
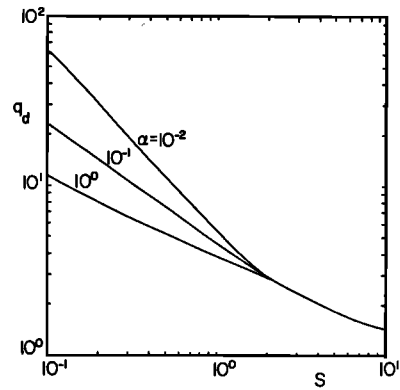

Fig. 4. Dominant growth rate factor q_d as a function of S for a range of α for hydrodynamic flow model. Unstable compression occurs over the entire range of S.

that deformation will actually be observed. The development of unstable deformation requires that the product of the rate of shortening and the time over which shortening has occurred is sufficient to produce structures of a discernible magnitude.

Figure 5 summarizes the relationships between λ_d/h, S, and α for viscous and plastic layer models. For a viscous layer, small S corresponds to large λ_d/h. This relationship is also predicted from flexural buckling theory for a strong viscous layer overlying a uniform viscous substrate as long as S is small [*Biot*, 1961]. At large S ($\gtrsim 10$), λ_d/h becomes independent of S in the hydrodynamic flow model, whereas in the flexural buckling model λ_d/h continues to decrease as S increases. The behavior in the flexural case is a consequence of the breakdown of the thin plate assumptions. For a plastic layer, λ_d/h is not strongly dependent on either S or α for the hydrodynamic flow model. Dominant wavelength is therefore nearly independent of the yield stress in the layer.

For a compressing viscous layer overlying a weaker substrate with uniform strength, both the hydrodynamic flow and flexural buckling formulations predict that λ_d/h increases as the ratio of layer to substrate strength increases. In the present model, which features a substrate in which strength varies exponentially, λ_d/h increases with increasing α. An increase in
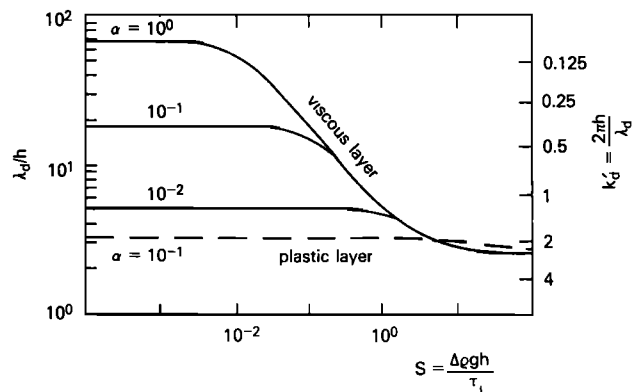

Fig. 5. The ratio λ_d/h as a function of S for a range of α for viscous and plastic strong layer rheologies for the hydrodynamic flow model. For the plastic case $n_1 = n_2 = 10^4$. For the viscous case the crustal layer is governed by the rheology of diabase [*Shelton and Tullis*, 1981] and the mantle layer is governed by the rheology of olivine [*Durham and Goetze*, 1977]. For both models the mantle substrate is governed by the rheology of olivine.

α represents a decrease in the strength contrast between the layer and substrate. A similar trend was found in a model of lithosphere extension by *Fletcher and Hallet* [1983]. This difference between the flexural and hydrodynamic models could have potentially important implications, as many previous studies have employed flexural approximations in lithosphere models.

Both q_d and k_d' vary with the stress exponents of the layer and substrate. Ductile rock deformation studies suggest that for geologically reasonable oceanic crustal and mantle constituents, n is between approximately two and five. In the present model, variations within that narrow range have a negligible effect on the growth rate. However, if the lithosphere contains a strong layer in which deformation is primarily brittle ($n \rightarrow \infty$), then q_d and therefore the degree of instability are much enhanced [*Fletcher and Hallet*, 1983; *Zuber et al.*, 1986]. The dependence of k_d' with n_1 is shown in Figure 5. Increasing n_1 decreases the dominant wavelength for most of the range of S.

Application to Indian Ocean Intraplate Deformation

We estimate the physical properties of the oceanic lithosphere on the basis of experimental rock mechanics studies and inferred compositional and thermal structures. The thickness of the crustal layer h_1 is taken as constant and equal to 6 km. In the viscous model the flow in the crustal and mantle layers, respectively, is governed by the rheologies of diabase [*Shelton and Tullis*, 1981] and olivine [*Durham and Goetz*, 1977]. In the plastic model both layers are described by a power law exponent $n = 10^4$. In both models flow in the mantle substrate is governed by the rheology of olivine. From Figure 5, which was constructed using these parameters, the thickness of the mechanically strong layer in the lithosphere can be estimated from the observed dominant wavelength. For example, a viscous layer with $\alpha = S = 0.1$ will deform with $\lambda_d/h = 13.7$. For a wavelength of deformation in the Indian Ocean of 186 km (see Figure 8), the inferred strong layer thickness is about 14 km. For $\alpha = 0.1$ and $S = 1$ and 10, λ_d/h values of 5.7 and 3.0 correspond to layer thicknesses of approximately 33 and 62 km, respectively.

Figure 5 was constructed assuming a crust to mantle layer strength ratio $R = 1$. If the oceanic crust is weaker than the underlying mantle, as suggested by experiments, then the lithosphere may be modeled as a weak layer overlying a stronger layer. A layer bounded on the top by a weaker layer and below by a weaker substrate may also be representative of a lithosphere which contains a strong central core [cf. *McAdoo and Sandwell*, 1985]. For the viscous case with $R < 1$, a larger value of λ_d/h results for a given S and α. For $R = 0.5$ and $\alpha = S = 0.1$, for example, $\lambda_d/h = 16$ and the corresponding strong layer thickness is 12 km. In this scenario, buoyancy forces influence the unstable flow to a lesser extent than for the case of a single layer of uniform strength.

Figure 6 illustrates the styles of deformation at the dominant wavelengths for the growth rate spectra in Figure 3b. These diagrams were constructed by calculating the perturbing flow at points on an initially rectangular grid and connecting the tips of the instantaneous velocity vectors. The fields shown were plotted for arbitrary strain rate and initial perturbation amplitudes and do not include the flow due to the basic state of compression.

Equation (14) shows that the absolute amplitude of interface deformation is proportional to the growth rate, the mean
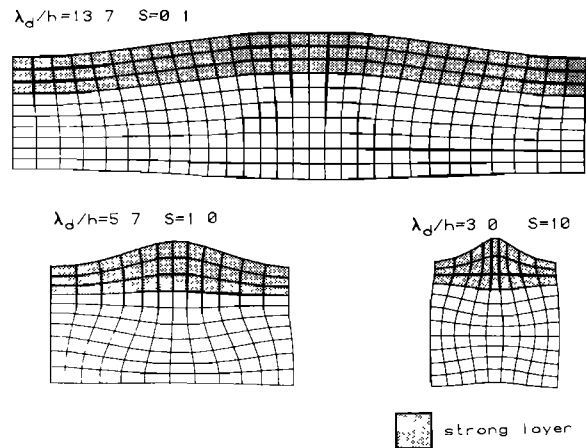

Fig. 6. Deformation due to perturbing flow associated with the growth rate spectra in Figure 3b. For $S = 0.1$ the strong layer of the lithosphere, designated by the shading, folds flexurally. For $S = 1$ and 10, deformation is characterized by nonuniform layer thickening which localizes in the vicinity of topographic highs. The style of deformation for $S = 1$ is folding and that for $S = 10$ is inverse boudinage. In all grids the basic state of uniform horizontal shortening has been removed so areas of apparent extension are in reality areas of minimum compression.

compression, and the amplitude of the initial disturbance. To explain a present topographic amplitude of 1 km in the Central Indian Basin given $\alpha = 0.1$, $R = 1$, and an estimated mean strain $\bar{\varepsilon}_{xx}t = 0.1$, initial disturbances of 0.12, 0.70, and 0.96 km, respectively, are required for a viscous layer with $S = 0.1$, 1, and 10. The negligible amplification of instability for large S argues against values in this range. If the strong layer is plastic, then the growth rate can provide the required amplification for large S and initial disturbances with magnitudes as small as a few tens of meters. Later analysis will show, however, that small λ_d/h characteristic of a plastic layer with any S or a viscous layer with large S is inconsistent with observational and experimental data on the mechanical structure of the oceanic lithosphere.

An arbitrarily strong layer ($S = 0$) deforms flexurally, in the antisymmetric or folding mode. In flexural folding deformation of the layer is manifest as bending, which arises from the unstable flow, accompanied by uniform thickening, which occurs due to the basic state of horizontal compression. The relative thickness of the deformed layer is nearly everywhere constant. The $S = 0.1$ case in Figure 6 represents a relatively strong lithosphere in which the layer, designated by the shading, and consequently the crust, which is a fraction of the strong layer, fold flexurally. In a weaker layer (larger S), buoyancy forces may become large enough to significantly influence the flow induced by the boundary conditions. With increasing S, λ_d/h decreases, and deformation is characterized by both uniform and nonuniform (localized) thickening, the latter of which is concentrated in areas of topographic upwarping. The wavelength to layer thickness ratio at which localized layer thickening ensues ($\lambda_d/h \cong 10$) corresponds approximately to that at which the hydrodynamic flow and flexural buckling models begin to deviate (see Figure 3). The amount of localized thickening increases progressively with increasing S. For the $S = 1$ case in Figure 6 and in general for $5 \lesssim \lambda_d/h \lesssim 9$, the layer folds nonflexurally. In an even weaker lithosphere the layer deforms by inverse boudinage in the symmetric or pinch-

and-swell mode. This occurs for $\lambda_d/h \lesssim 4$ and is exemplified by the $S = 10$ case in Figure 6. A lithosphere consisting of a weak viscous layer overlying a stronger viscous layer requires a larger S value to produce an amount of nonuniform thickening equivalent to that shown in the latter two cases in Figure 6. For a given buoyancy force, deformation by nonflexural folding or inverse boudinage requires a lithosphere which is weaker than that for these cases.

Localized thickening of the strong layer arises from the flow associated with unstable deformation. Therefore crustal thickness variations associated with the deformation are dynamically produced and need not isostatically compensate the surface topography. In fact, none of the model lithospheres shown in Figure 6 have developed a compensating crustal root. Flexural folding of the crust such as shown for the $S = 0.1$ case has been suggested as the mechanism of intraplate deformation on the basis of gravity anomalies from the Seasat altimeter data [*Weissel and Haxby*, 1982]; however, the model results show that uncompensated crustal thickening characteristic of larger S cannot be ruled out. To distinguish between the various styles of deformation illustrated in Figure 6 requires careful consideration of the geophysical and structural signatures of the Indian plate and evidence of lithospheric structure from rock mechanics.

DISCUSSION

Constraints on Strong Layer Thickness

Figure 7 shows the depth distribution of intraplate seismicity in the Central Indian Basin and an experimentally derived compressive strength envelope for 55 Ma oceanic lithosphere, the average age at the onset of intraplate deformation. From this we attempt to place constraints on the thickness of the strong layer. The depth distribution of intraplate earthquakes provides a clear measure of the range over which large deviatoric stresses are accumulated and presently provides the best observational constraint on the thickness of the mechanically strong part of the lithosphere. On the basis of Figure 7, an upper limit of h could be the depth below which earthquakes cease to occur, and strength is negligible compared to its value at the brittle-ductile transition defined by the strength envelope; this occurs at a depth of about 40 km. On the other

hand, the absence of shallow earthquakes and the low near-surface brittle strength shown in Figure 7 combined with observations of extensive shallow faulting of oceanic crust in this area [cf. *Weissel et al.*, 1980; *Geller et al.*, 1983] suggest that the upper part of the lithosphere is relatively weak and perhaps should not be included as part of the strong layer. If defined on the basis of the depth range of the most extensive seismicity, then h could be as little as 10 km. On the basis of model results, if $20 \lesssim h \lesssim 40$ km then deformation should be characterized by folding with periodic layer thickening, whereas if $10 \lesssim h \lesssim 20$ km then flexural folding is preferred. Inverse boudinage of the strong layer, which requires $h \gtrsim 50$ km, is not supported by either seismological or rheological data. The broad peak in the growth rate spectrum characteristic of large S and small λ_d/h (see Figure 3) provides an additional argument against the regular development of structures in a strong layer which falls in this thickness range.

Role of Sediments

A fundamental question is whether sediments from the Bengal and Nicobar Fans controlled the style and extent of intraplate deformation or the deformation controlled the distribution of sediments. Seismic reflection profiles show that sediments associated with the northernmost topographic undulations are deformed along with the oceanic crust, indicating their presence throughout intraplate deformation. However, in the south topographic undulations, geoid and gravity anomalies, intraplate earthquakes, and anomalously high heat flow are observed to extend beyond the distal edges of the Bengal and Nicobar Fans, indicating that at least part of the deformation is spatially unrelated to sedimentation. Figure 5 illustrates that decreasing the buoyancy force at the top of the crust due to sediment loading increases λ_d/h for a viscous layer over the range where the curves slope. For the appropriate range of S, a viscous layer of constant strength and thickness would exhibit a longer wavelength of deformation in areas which were initially overlain by sediments. The increase in dominant wavelength due to sediment loading has also been shown by *McAdoo and Sandwell* [1985] for elastic-plastic buckling. In the present model for a plastic layer, λ_d/h is constant for all S, and the wavelength would be expected to be the same in initially sedimented and unsedimented regions.

To examine whether wavelength varies with location, we measured the spacings of adjacent maxima and minima of deflections of the vertical calculated from Seasat-derived geoid anomalies which correlate with undulations in the basement topography. Peak-to-peak and trough-to-trough spacings of the deflections measured in the manner of *McAdoo and Sandwell* [1985] are shown in Figure 8. The top histogram illustrates that the measured wavelengths range from about 100 to 300 km with a mean of 186 km. The bottom histograms show the sample broken into three latitude bins. Note that the mean spacing increases to the north, as would be expected if at the onset of deformation sediments were present in the north but not in the south. The difference in the means of the southernmost and northernmost bins is over 50 km, which is more than a factor of 5 greater than that which would be expected if the difference were attributable solely to the thickening of oceanic lithosphere with age in this region. If due to a change in S, the observed variation in wavelength could also be explained by lateral inhomogeneities in the strength or thickness of the layer. However, these explanations are not supported by
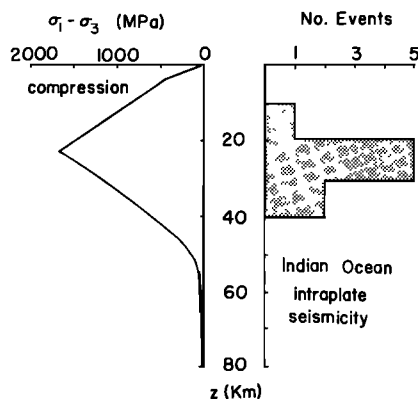
Fig. 7. (left) Compressive yield envelope for 55 Ma oceanic lithosphere assuming $\bar{\varepsilon}_{xx} = 10^{-15}$ s^{-1}, zero pore pressure, and a dry olivine flow law from *Brace and Kohlstedt* [1980]. (right) Depth distribution of intraplate seismicity in the Central Indian Basin. Focal depths were compiled from *Bergman and Solomon* [1980, 1985], *Stein and Weissel* [1984], and *Wiens and Stein* [1983]. Note the absence of shallow seismicity.
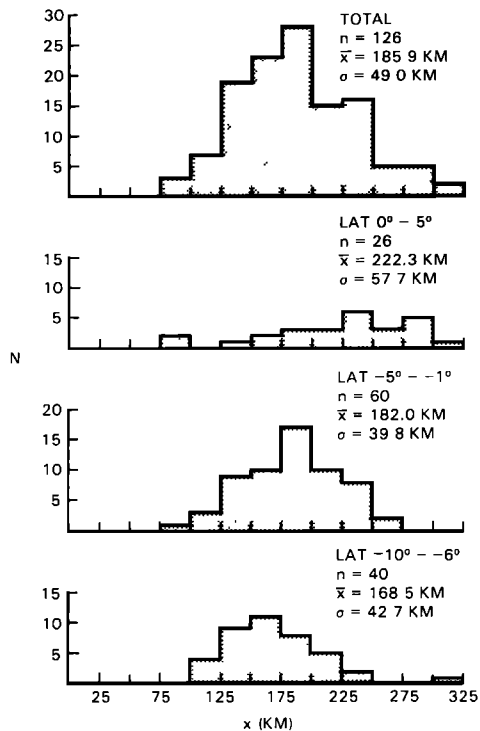
Fig. 8 Spacings of Seasat-derived geoid anomalies associated with basement deformation The top histogram shows spacings in range -10 to $+5$ latitude and 75°E to 85°E longitude. The bottom histograms show spacings broken into three latitude bins. Note that the mean spacing increases from south to north. Implications are discussed in the text.

TABLE 1. Layer Strengths

S	λ_d, km	λ_d/h, hour	h, km	τ, MPa No Sediments	τ, MPa Sediments
0.1	222	13.7	16.2	3176	1111
	182	13.7	13.3	2607	912
	168	13.7	12.3	2411	844
1.0	222	5.7	39.0	764	268
	182	5.7	31.9	625	219
	168	5.7	29.5	578	202
10.0	222	3.0	74.0	145	51
	182	3.0	60.6	119	42
	168	3.0	56.0	110	38

observations of heat flow and the depth distribution of intraplate seismicity, which do not show a marked North-South variation in the region within which the geoid spacings were measured.

From Figure 5 and the observed range of wavelengths we can place broad estimates on the level of stress in the Indian plate during the early stages of intraplate deformation. Table 1 lists thickness-averaged compressive layer stresses for the S and λ_d/h values examined in this study. Results are shown for cases in which the crustal layer ($\rho_1 = 3.0$ g cm^{-3}) is initially covered by sediments ($\rho_0 = 2.3$ g cm^{-3}) and water ($\rho_0 = 1.0$ g cm^{-3}). Note that if sediments were present, the layer strength indicated by the dominant wavelength is almost a factor of 3 less than if the area was initially devoid of a sediment cover. For $S = 0.1$ and in the absence of sediments, layer strengths are comparable to the elastic buckling stress and are in excess of experimental estimates of the strength of the lithosphere. If sediments were present, stresses are still high but are more compatible with experimental results. For $S = 1$, the model predicts stresses in the approximate range 200–800 MPa, and for S = 10, stresses range from approximately 40–150 MPa. However, as was discussed previously, the range of layer thicknesses predicted by the observed wavelengths for $S = 10$ is inconsistent with seismic and rheological data; therefore the associated range of stresses is unlikely. A range of model results thus suggests stresses in the Central Indian Basin in the broad range of several hundreds of MPa. This is consistent with the elastic-plastic buckling stress of 600 MPa [McAdoo and Sandwell, 1985] and with a numerical estimate of the regional stress in the Indian Plate of about 400 MPa [Cloetingh and Wortel, 1985].

Observations of the spatial distribution of crustal thickness in the Central Indian Basin will permit better constraints on the strength of the lithosphere. If deformation is occurring by flexural folding indicative of a strong lithosphere, then the crust should exhibit almost constant thickness beneath both topographic highs and lows. If instead the lithosphere is weaker and folding is characterized by periodic layer thickening, then the crust beneath topographic highs may be considerably thicker than that beneath topographic lows. For example, the crust for the $S = 1$ case in Figure 6 is thickened by about 30%.

In the region of intraplate deformation sediments on a local scale are often ponded in topographic depressions. If sediments were present in isolated patches at the onset of deformation, they would have acted as an irregularly distributed load and deflections associated with the loading would have magnified during compression. The amplification of the initial deflections is governed by the wave number spectrum of the load, the mechanical properties of the lithosphere, and the magnitude of the compression. In this scenario an initial sediment load would control in part the growth and spacing of the basement undulations. Lambeck [1983] solved a flexural buckling problem for a viscoelastic lithosphere with an initial irregularly distributed surface load and showed how the presence of initial deflections allows deformation to occur at stresses much less than the elastic buckling stress. The regular spacing of topographic undulations in the Indian Ocean indicates that if the intraplate deformation is a consequence of the amplification of an initial load, then this load must have been distributed approximately periodically. In the hydrodynamic flow model, stress levels can be in agreement with experimental predictions without invoking a quasi-periodic initial load. An overlying layer of weak sediments will increase the growth rate and dominant wavelength, but surface deflections due to an initial sediment load are not required to initiate deformation.

Relationship of Tectonic Setting to Deformation

Another documented region of large-scale intraplate deformation of the ocean floor occurs in the area of the Azores-Gibraltar plate boundary [Grimison and Chen, 1986]. Like the Central Indian Basin, this region exhibits scattered, deep earthquakes, complex bathymetry, and large gravity and geoid anomalies. As most of the oceanic lithosphere is in a state of net compression, the question arises as to why intraplate deformation has developed in these regions and not in others. With regard to the Central Indian Basin, we invoke the suggestions of Weissel et al. [1980] and Cloetingh and Wortel

[1985] that the unique tectonic setting of the Indian plate may have played an important role in determining the level of intraplate stress. North of the region of intraplate deformation the Indian subcontinent collides with Asia along the Himalaya. East of the Ninetyeast Ridge, which is undergoing left-lateral strike-slip motion [Stein and Okal, 1978], the Indian plate subducts along the Sunda Arc. Cloetingh and Wortel [1985] have noted that variations of the age of the subducting plate may cause significant variations in the slab pull force along this boundary. The distribution of forces arising from the unusual plate geometry in the Central Indian Basin may have allowed stresses to concentrate at levels required for intraplate deformation.

CONCLUSIONS

We consider flexural buckling and the hydrodynamic growth of small-amplitude instabilities as mechanisms for compressional intraplate deformation of oceanic lithosphere. In both models the lithosphere is treated as a strong layer overlying a half space in which strength decreases exponentially with depth. In the flexural buckling model the layer and half space are assumed to be viscous, and deformation of the layer occurs in the antisymmetric mode by flexural folding. This model is applicable for deformation in the limit of a strong layer, or equivalently, a large wavelength to layer thickness ratio ($\lambda_d/h \gtrsim 10$). In the hydrodynamic flow model a range of deformational styles are possible. In the viscous case, deformation of the layer in a strong lithosphere occurs by flexural folding at a wavelength which agrees with that predicted from flexural buckling theory. In a lithosphere of intermediate strength, deformation of the layer is characterized by folding accompanied by periodic layer thickening. In a weak lithosphere the layer deforms by inverse boudinage in the symmetric or pinch-and-swell mode. If the layer has a plastic rheology, the style of deformation is independent of the yield stress; deformation in all cases occurs by inverse boudinage. The characteristics of both flexural and nonflexural folding are generally consistent with the observed seismicity in the Central Indian Basin and with results from experimental rock deformation studies. Inverse boudinage of either a viscous or plastic layer requires a layer thickness greater than 50 km, which is in excess of that suggested by observations and experiments.

If sediments were present at the onset of intraplate deformation, then the layer strength required to explain the dominant wavelength is almost a factor of three less than if the area was initially sediment-free. For a range of plausible models which consider both a sediment-covered and sediment-free lithosphere, compressive layer strengths of several hundreds of MPa are implied for the Indian plate. On the basis of predicted stress magnitudes and the areal distributions of basement undulations and sediments, the results suggest that a weak layer of sediments overlying the oceanic crust would have facilitated the development of intraplate deformation, but need not have been present for deformation to initiate.

REFERENCES

Bergman, E. A., and S. C. Solomon, Oceanic intraplate earthquakes: Implications for local and regional intraplate stress, *J. Geophys. Res., 85,* 5389–5410, 1980.

Bergman, E. A., and S. C. Solomon, Earthquake source mechanisms from body-waveform inversion and intraplate tectonics in the Northern Indian Ocean, *Phys. Earth Planet. Inter., 40,* 1–23, 1985.

Biot, M. A., Theory of folding of stratified viscoelastic media and its implications in tectonics and orogenesis, *Geol. Soc. Am. Bull., 72,* 1595–1620, 1961.

Bodine, J. H., M. S. Steckler, and A. B. Watts, Observations of flexure and the rheology of the oceanic lithosphere, *J. Geophys. Res., 86,* 3695–3707, 1981.

Brace, W. F., and D. L. Kohlstedt, Limits on lithospheric stress imposed from laboratory experiments, *J. Geophys. Res., 85,* 6248–6252, 1980.

Cloetingh, S., and R. Wortel, Regional stress field of the Indian Plate, *Geophys. Res. Lett., 12,* 77–80, 1985.

Davis, E. E., and C. R. B. Lister, Fundamentals of ridge crest topography, *Earth Planet. Sci. Lett., 21,* 405–413, 1974.

Durham, W. B., and C. Goetze, A comparison of creep properties of pure forsterite and iron bearing olivine, *Tectonophysics, 40,* 15–18, 1977.

Fletcher, R. C., Folding of a single viscous layer: Exact infinitesimal amplitude solution, *Tectonophysics, 39,* 593–606, 1977.

Fletcher, R. C., and B. Hallet, Unstable extension of the lithosphere: A mechanical model for Basin and Range structure, *J. Geophys. Res., 88,* 7457–7466, 1983.

Geller, C. A., J. K. Weissel, and R. N. Anderson, Heat transfer and intraplate deformation in the Central Indian Ocean, *J. Geophys. Res., 88,* 1018–1032, 1983.

Goetze, C., and B. Evans, Stress and temperature in the bending lithosphere as constrained by experimental rock mechanics, *Geophys. J. R. Astron. Soc., 59,* 463–478, 1979.

Grimison, N. L., and W.-P. Chen, The Azores-Gibraltar plate boundary: Focal mechanisms, depths of earthquakes, and their tectonic implications, *J. Geophys. Res., 91,* 2029–2047, 1986.

Kirby, S. H., Rheology of the lithosphere, *Rev. Geophys., 21,* 1458–1487, 1983.

Lambeck, K., Structure and evolution of the intracratonic basins of central Australia, *Geophys. J. R. Astron. Soc., 74,* 843–866, 1983.

McAdoo, D. C., and D. T. Sandwell, Folding of oceanic lithosphere, *J. Geophys. Res., 90,* 8563–8569, 1985.

Ricard, Y., and C. Froidevaux, Stretching instabilities and lithospheric boudinage, *J. Geophys. Res., 91,* 8314–8324, 1986.

Richardson, R. M., S. C. Solomon, and N. H. Sleep, Tectonic stress in the plates, *Rev. Geophys., 17,* 981–1019, 1979.

Shelton, G., and J. Tullis, Experimental flow laws for crustal rocks, *Eos Trans. AGU, 62,* 396, 1981.

Smith, R. B., Unified theory of the onset of folding, boudinage, and mullion structure, *Geol. Soc. Am. Bull., 86,* 1601–1609, 1975.

Smith, R. B., Formation of folds, boudinage, and mullions in non-Newtonian materials, *Geol. Soc. Am. Bull., 88,* 312–320, 1977.

Stein, C. A., and J. K. Weissel, Constraints on the Central Indian Ocean thermal structure from depths of seismicity and basement, *Eos Trans. AGU, 65,* 245, 1984.

Stein, S., and E. A. Okal, Seismicity and tectonics of the Ninetyeast Ridge area: Evidence for internal deformation of the Indian plate, *J. Geophys. Res., 83,* 2233–2246, 1978.

Sykes, L. R., Seismicity of the Indian Ocean and a possible nascent island arc between Ceylon and Australia, *J. Geophys. Res., 75,* 5041–5055, 1970.

Timoshenko, S. P., and S. Woinowsky-Krieger, *Theory of Plates and Shells,* 580 pp., McGraw-Hill, New York, 1959.

Weissel, J. K., and W. F. Haxby, Predicting seafloor topography from Seasat altimeter data using isostatic models, *Eos Trans. AGU, 63,* 907, 1982.

Weissel, J. K., R. N. Anderson, and C. A. Geller, Deformation of the Indo-Australian plate, *Nature, 287,* 284–291, 1980.

Wiens, D. A., and S. Stein, Age dependence of oceanic intraplate

seismicity and implications for lithospheric evolution, *J. Geophys. Res.*, *88*, 6455–6468, 1983.

Wiens, D. A., et al., A diffuse plate boundary model for Indian Ocean Tectonics, *Geophys. Res. Lett.*, *12*, 429–432, 1985.

Zuber, M. T., E. M. Parmentier, and R. C. Fletcher, Extension of continental lithosphere: A model for two scales of Basin and Range deformation, *J. Geophys. Res.*, *91*, 4826–4838, 1986.

M. T. Zuber, Geodynamics Branch, NASA Goddard Space Flight Center, Greenbelt, MD 20771.